Available online at www.sciencedirect.com
SCIENCE DIRECT®
Journal of Sound and Vibration 260 (2003) 141–165
JOURNAL OF SOUND AND VIBRATION
www.elsevier.com/locate/jsvi

Vibration and buckling of flat free–free plates under non-uniform in-plane thermal stresses

D.J. Mead*

Institute of Sound and Vibration Research, University of Southampton, Highfield, Southampton, UK SO 1BJ

Received 14 November 2001; accepted 11 March 2002

Abstract

Detailed consideration is given to the modes and frequencies of a free rectangular Kirchoff plate subjected to in-plane stresses generated by prescribed non-uniform surface temperature distributions which are doubly symmetrical about the plate central axes. Physical understanding is sought of phenomena observed by previous investigators. Stress distributions corresponding to three different temperature distributions have first been studied and incorporated in a Rayleigh Ritz analysis to find natural frequencies and modes. All frequencies change as the temperature changes, some much more than others. All eventually vanish, one after the other, as the temperature reaches certain critical positive and negative values at which the plate goes into statically unstable buckling modes. Whether the frequencies rise or fall with rising temperature at the plate centre depends on the relative magnitudes of pairs of positive and negative critical temperatures. The modes of buckling at each pair of critical temperatures may differ greatly from one another and also from the vibration modes at zero temperature. The relationship between the square of the frequency and the temperature is then no longer approximately linear, although it is exactly so for certain simple in-plane stress distributions. Conditions have nevertheless been identified under which it is a very good approximation to the actual frequencies of the heated plate over wide temperature ranges.

1. Introduction

The natural frequencies of beams and plates, both flexural and torsional, have long been known to vary with the axial load or in-plane stress which is acting [1]. Overall compressive loads or stresses reduce the frequencies while tensile loads or stresses increase them. If the boundary conditions of the plate or beam are such that its critical buckling modes are the same as the natural modes of vibration, the natural frequency $\omega_{n,0}$ at zero load and its value $\omega_{n,P}$ under

*Tel.: +44-23-8059-2314; fax: +44-23-8059-3241.
E-mail address: denysmead@aol.com (D.J. Mead).

0022-460X/03/$ - see front matter
PII: S0022-460X(02)00919-7

compressive load P are related by the simple linear law $\omega_{n,P}^2 = \omega_{n,0}^2(1 - P/P_{crit,n})$ [1,2]. $P_{crit,n}$ is the nth critical buckling load of the structure at which the buckling mode is the same as the nth natural mode of vibration. As the compressive load approaches the lowest critical buckling load, the fundamental natural frequency approaches zero.

If the axial loads are caused by restraints to thermal expansion, they are proportional to the temperature T which causes this expansion. Under the same assumptions as above, the simple linear law then becomes $\omega_{n,0}^2 = \omega_{n,P}^2(1 - T/T_{crit,n})$. $T_{crit,n}$ is now the nth critical buckling temperature which causes buckling in the same nth mode. The equation is still true if the load or temperature become negative. The force on the structure is now tensile and the frequency continues to rise as it increases.

Real structures under quite simple static loads have some members under compression and some under tension. The natural frequencies of simple beams and redundant frameworks in this condition have been considered by the author [3]. A free redundant framework with no external loads acting has loads in its members when their individual thermal strains are unequal. A flat uniform plate has non-uniform thermal in-plane strains when its surface temperature is non-uniform thereby causing compressive in-plane stresses in some parts of the plate and tensile stresses elsewhere. It will buckle at certain negative and positive critical temperatures whether or not any external loads are acting. The natural frequencies change with changing temperature so the question is "In which direction? Up or down, and why? Why does the simple linear law break down, and to what extent?". This paper seeks to answer these questions for a flat rectangular plate, free on all four sides and under three simple non-uniform surface temperature distributions.

Many papers have been published on the effects of different in-plane stress systems on plate flexural vibrations. In his classic monograph Leissa [4] identified 24 such papers before 1969. Subsequently (with Simons [5]), he studied their influence on cantilever plate vibration when the stresses derive from uniform in-plane inertia loads generated by a uniform in-plane acceleration of the plate. A simple Airy stress-function problem had first to be solved to relate the stresses to the applied acceleration, and these stresses were then incorporated into the total potential energy function for the vibrating plate. A Rayleigh–Ritz analysis was then used to find the flexural frequencies, the transverse plate deflection being represented approximately by a product series of appropriate beam-function modes, i.e., the vibration eigenfunctions of uniform beams with boundary conditions corresponding to those of the plate. This has been the approach in much of the subsequent work in the same subject area. Unsurprisingly, Leissa and Simons found that the fundamental frequency of the plate dropped when the inertia forces compressed the plate but increased when the forces stretched the plate. Sufficient compression reduced the frequency to zero.

Dickinson [6] studied plates with pre-assigned uniform or uniformly varying in-plane stresses and therefore did not have a stress function problem to solve. Otherwise he used the same energy approach as Leissa. Simply supported, fully clamped and cantilevered plates were considered. The linear law was clearly shown to be inapplicable when a uniform shear stress acts on the plate. This is to be expected, as positive and negative shear stresses on a rectangular plate must both have the same effect on a natural frequency. The gradient of ω_P^2 versus shear stress at zero shear stress must therefore be zero, not the non-zero constant of the linear law. Moreover, the plate can buckle and lead to a zero natural frequency at a pair of equal and opposite critical shear stress values. Between these, ω_P^2 must vary in a 'somewhat' parabolic form, not linearly.

The same argument applies to a direct stress distribution which varies linearly across the plate through zero along a symmetry axis but which remains the same along the plate. (This would be generated by a constant applied in-plane bending moment.) Using a finite element method, Mei and Yang [7] studied the effect of this stress system on the vibration of a simply supported plate and demonstrated the inapplicability of the linear law to this stress condition, although it is valid for a uniform compressive stress.

Commenting on Ref. [7] Dawe [8] pointed out that while the linear law might sometimes appear to hold at low stress levels, it can mislead at higher values. He also showed how the vibration modes (as well as the frequencies) of a clamped plate can vary with increasing uniform compressive stress level.

Plates which are completely free along all four edges were considered by Porter Goff [9] and Kaldas and Dickinson [10,11] all of whom considered a single rectangular plate with a weld line along its centre. Kaldas and Dickinson also considered plates with edge welds formed by a line of weld material deposited along the edges. In all of these cases, the welding process left residual in-plane tensile stresses in the plate, near to and in the direction of the weld-line. Residual compressive stresses existed outside that region together with an associated system of shear stresses all over the plate. The free plates were therefore subjected simultaneously to a symmetrical self-equilibriating system of compressive and tensile stress and an antisymmetrical system of shear stress. Natural frequencies computed for the different but specific plates with their own specific stress fields were compared with experimentally measured values. Some of these were higher, but most were lower than those of the corresponding unstressed plate. No explanations were advanced and the effect of increasing or decreasing the stress level was not studied. Comparison with a linear law could not be made nor was it necessary for the purposes of their studies. Centrally welded plates of two different aspect ratios were also considered in Refs. [10,11].

Apart from Refs. [9–11], the only paper considering the free–free plate is the significant work of Bailey [12]. He considered a family of eight uniform square plates with different boundary conditions. One plate was free along all of its boundaries. Six plates were exposed experimentally to non-uniform temperature distributions, and two (including the free–free plate) to a theoretical 'cubic-constant' distribution (i.e., $T(x, y) = T_0|y^3|$; y is the distance from the plate longitudinal centreline). Measured and calculated frequencies were found to agree quite well. Reissner's energy functional was used to set up the computational programme in two stages: (a) to find the internal in-plane stresses from the stress function corresponding to the particular temperature distribution and (b) to find the frequencies of the plate when subjected to these stresses. The stress function and plate transverse deflection were represented by different double series of products of appropriate beam-function modes.

Calculation and experiment alike showed some of the modal frequencies to increase while others decreased. The simple linear law appeared to work for some modes but certainly not for others. No explanations were sought and the temperature range considered was not extensive. The free–free plate under the cubic-constant temperature distribution was only allowed a positive increase in temperature such that the plate was always hotter along two opposite edges than at its centre. The reverse situation (hotter at the centre than at the edges) was not considered. The temperature range did not therefore encompass the lowest positive and lowest negative critical temperatures which identify the boundaries of the range for static plate stability.

Free–free plate boundary conditions are, of course, the most impractical and unusable of all the possible boundary conditions, except for vibration demonstrations to students! Serious researchers nevertheless have long been fascinated by them—especially square ones with their *penchant* for degenerate modes! (see Refs. [13–15] and the work of many others listed by Leissa [4]). In the present context of self-equilibriating thermal stresses, one might question why such stress systems change the frequencies of a free–free plate at all. As the plate deflects in a given mode, the internal compressive stresses do positive internal work and the tensile stresses do negative work. If the compressive and tensile stresses are self-equilibriating, why do these work increments not cancel out and leave the total potential energy unchanged? And why do some frequencies go up and some go down with change of temperature? This current study addresses these questions.

It will be shown that the dynamic behaviour of the plate in the narrow temperature range of static plate stability can be better understood by studying a much wider range which extends to the higher critical buckling temperatures. It will also be shown that understanding the actual thermal stress distribution leads to an understanding of its effect on plate modes and frequencies. It is also helpful to study rectangular plates with aspect ratios other than that of Bailey's square plate which has some unique features.

The theoretical and computational methods employed in this paper are not new. Basically it is that of Simons and Leissa [5] and Bailey [12] in which the solution of a thermal stress-function problem precedes a Rayleigh–Ritz vibration analysis. The same approach had been used long before in solving thermal buckling problems (see Ref. [16]), and this was followed initially in the work of the current paper.

2. The thermal stresses

2.1. The stress equations

Consider the flat, uniform and rectangular plate of Fig. 1 with the length, breadth and thickness of a, b and h, respectively. It is subjected to the temperature distribution $T(x, y)$ which is constant through the plate thickness but varies over the plate surface. Provided no thermal transverse

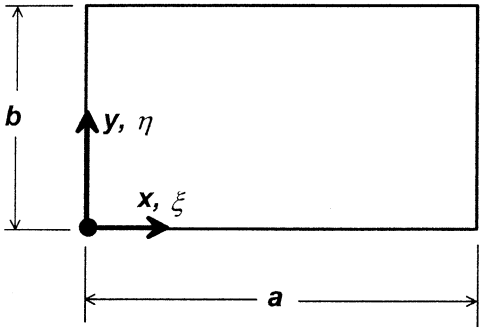

Fig. 1. The flat rectangular plate; dimensions and co-ordinate system.

buckling occurs, the resulting in-plane direct and shear stresses constitute a generalized plane stress system governed by the Airy stress function ϕ [16]. The stresses are then found from

$$\sigma_x = \frac{\partial^2 \phi}{\partial y^2}, \tag{1a}$$

$$\sigma_y = \frac{\partial^2 \phi}{\partial x^2}, \tag{1b}$$

$$\sigma_{xy} = -\frac{\partial^2 \phi}{\partial x \partial y}, \tag{1c}$$

where ϕ is the solution of the bi-harmonic equation

$$\nabla^4 \phi = -E\alpha \nabla^2 T(x, y), \tag{2}$$

∇^2 is the Laplace operator $(\partial^2/\partial x^2 + \partial^2/\partial y^2)$, ∇^4 is the bi-harmonic operator $(\partial^2/\partial x^2 + \partial^2/\partial y^2)^2$, E is Young's modulus of the plate material and α is its coefficient of linear expansion.

ϕ must be found such that the boundary conditions of stress and displacement at the edges of the plate are satisfied. This paper will be concerned only with a plate which is stress-free on all edges so there are no edge-displacement restrictions. Hence, according to Eqs. (1a)–(1c) ϕ must satisfy

$$\frac{\partial^2 \phi}{\partial y^2} = 0 \quad \text{at } x = \pm a/2, \tag{3a}$$

$$\frac{\partial^2 \phi}{\partial x^2} = 0 \quad \text{at } y = \pm b/2, \tag{3b}$$

$$\frac{\partial^2 \phi}{\partial x \partial y} = 0 \quad \text{at } x = \pm a/2, \ y = \pm b/2. \tag{3c}$$

This thermal stress problem was solved long ago by Przemieniecki [17] (and later by Bassily and Dickinson [18]) for a particular parabolic temperature distribution by representing ϕ in the generalized and truncated Fourier double-series form

$$\phi(x, y) = \sum_{m=1}^{M} \sum_{n=1}^{N} A_{mn} f_m(x) g_n(y). \tag{4}$$

For the functions $f_m(x), g_n(y)$ they took the characteristic ortho-normal beam functions of the free vibration modes of a uniform clamped–clamped beam. By virtue of these functions each product term within series (4) satisfies the three stress boundary conditions of Eqs. (3a)–(3c) for the free–free plate, so the whole stress function expressed in this form satisfies all the stress boundary conditions for the plate.

The A_{mn}'s of Eq. (4) are found from a set of $(N \times M)$ linear equations established by minimizing the total plate energy as a function of ϕ. Alternatively, they may be derived (following Przemieniecki) by substituting Eq. (4) into Eq. (2), multiplying both sides of the equation in turn by $g_m(x)h_n(y)$ $(m = 1\text{–}M, n = 1\text{–}N)$ and then by integrating the whole product over the surface of the plate. The two methods gives the same result.

The number of integrals which actually have to be evaluated for the left-hand side of the equations for the A_{mn}'s is greatly reduced by virtue of the orthogonal properties of the beam functions. For the right-hand side, $T(x,y)$ should be expressed in the form $T_0 t(x,y)$, T_0 being the reference temperature at a point on the plate where $T(x,y)$ has unit value.

With M modes used for the stress function in the x direction and N in the y direction, the total number of product modes and A_{mn}'s is $(N \times M)$ and the A_{mn}'s are found from the linear equations

$$[\mathbf{C}]\{\mathbf{A}_{mn}\} = -E\alpha T_0\{\mathbf{RHS}\}. \tag{5}$$

Expressions for the general element of the square matrix [**C**] (with $(N \times M)^2$ elements) and the column matrix {**RHS**} (with $(N \times M)$ elements) are given in Appendix A. In terms of the A_{mn}'s and the $g(x)$, $h(y)$ functions, the stresses are now found from

$$\sigma_x(x,y) = \sum_{m=1}^{M}\sum_{n=1}^{N} A_{mn} f_m(x) g_n''(y), \tag{6a}$$

$$\sigma_y(x,y) = \sum_{m=1}^{M}\sum_{n=1}^{N} A_{mn} f_m''(x) g_n(y), \tag{6b}$$

$$\tau_{xy}(x,y) = -\sum_{m=1}^{M}\sum_{n=1}^{N} A_{mn} f_m'(x) g_n'(y), \tag{6c}$$

in which $'$ and $''$ represent, respectively, the first and second derivatives of the functions with respect to their own independent variables.

2.2. Computed thermal stresses

Calculations have been performed for a plate of aspect ratio $a/b = 2.0$, free on all four edges and subjected in turn to the following different symmetrical temperature distributions:

(1) A one-dimensional parabolic distribution with the temperature varying parabolically across the width of the plate, i.e., $T(\xi,\eta) = T_0 4(\eta - \eta^2)$; this has its maximum of T_0 along the plate centreline, $\eta = 1/2$.
(2) A two-dimensional parabolic distribution with the temperature varying parabolically over both width and length of the plate, i.e., $T(\xi,\eta) = T_0 4(\eta - \eta^2)4(\xi - \xi^2)$; this has its maximum of T_0 at the plate centre.
(3) A uniform temperature T_0 over the central rectangular portion of the plate enclosed by $\frac{1}{4} < \xi < \frac{3}{4}, \frac{1}{4} < \eta < \frac{3}{4}$; elsewhere the temperature is zero.

The double symmetry of each of these distributions means that the modes used in the stress function products need only be the symmetric (odd-numbered) beam functions. Accordingly, the six beam functions ($m = 1, 3, 5, 7, 9, 11$) were used for ϕ in the (long) ξ direction, and four ($n = 1, 3, 5, 7$) were used in the (short) η direction. Twenty-four different product modes were therefore used.

Fig. 2 shows the variation over the plate surface of the computed non-dimensional direct and shear stresses $\sigma_x/E\alpha T_0$, $\sigma_y/E\alpha T_0$, $\tau_{xy}/E\alpha T_0$ generated by temperature distribution (1). The central region of the plate is compressed in both x and y directions (σ_x and σ_y are both negative) whilst

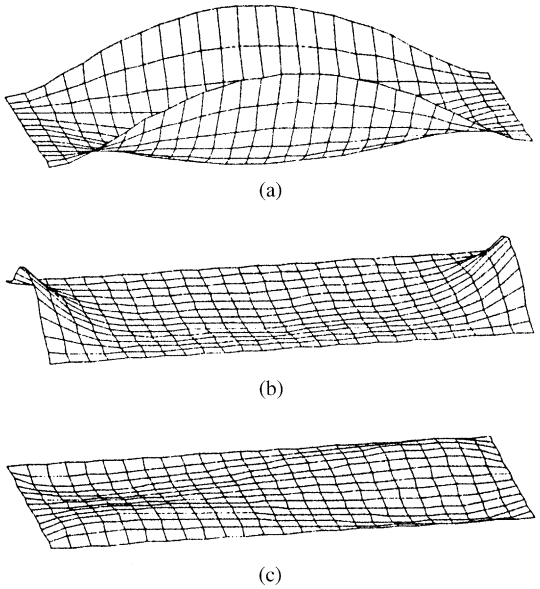

Fig. 2. The variation over the plate surface of the computed ND stresses for the two-dimensional parabolic temperature distribution. Plate aspect ratio = 2: (a) σ_x, (b) σ_y and (c) τ_{xy}.

parallel to and near the plate edges the direct stresses are tensile (positive). Normal to each edge the direct stresses are necessarily zero. The direct stress distributions are both doubly symmetric about the two plate centrelines whereas the shear stress is doubly antisymmetric. The general forms and magnitudes of all these stresses are closely similar to those found for the same temperature distribution by some of the earliest workers [17,19]. With the poor calculating facilities of those days, they had to use far fewer product modes so the current work must be more accurate.

Figs. 3(a)–(f) compare the direct stresses along the plate centrelines generated by the three different temperature distributions. Distributions (1) and (2) create very similar stress patterns, distribution (2) generating marginally higher compression near the plate centre. At first sight, this might seem to be surprising as distribution (1) has a higher average temperature over the whole plate. However, the right side of Eq. (2) shows that the property of the temperature distribution which governs the magnitude of the stress function is not its average value but its second derivatives in both x and y directions. Both distributions have the same second derivatives in the y direction but the x-wise second derivative for distribution (1) is zero whereas it is non-zero for distribution (2). This leads to the increased direct stresses for (2).

The increased compressive stress σ_x along the centreline near the plate centre (cf., Figs. 3(c) and (a)) is necessarily accompanied by the increased tensile stress σ_x at the plate edges (cf., locations 0 and 1 in Figs. 3(b) and (d)).

The stress distribution generated by temperature distribution (3) is significantly different from that of (1) or (2), and the magnitudes are substantially larger, albeit over small regions. Again, this

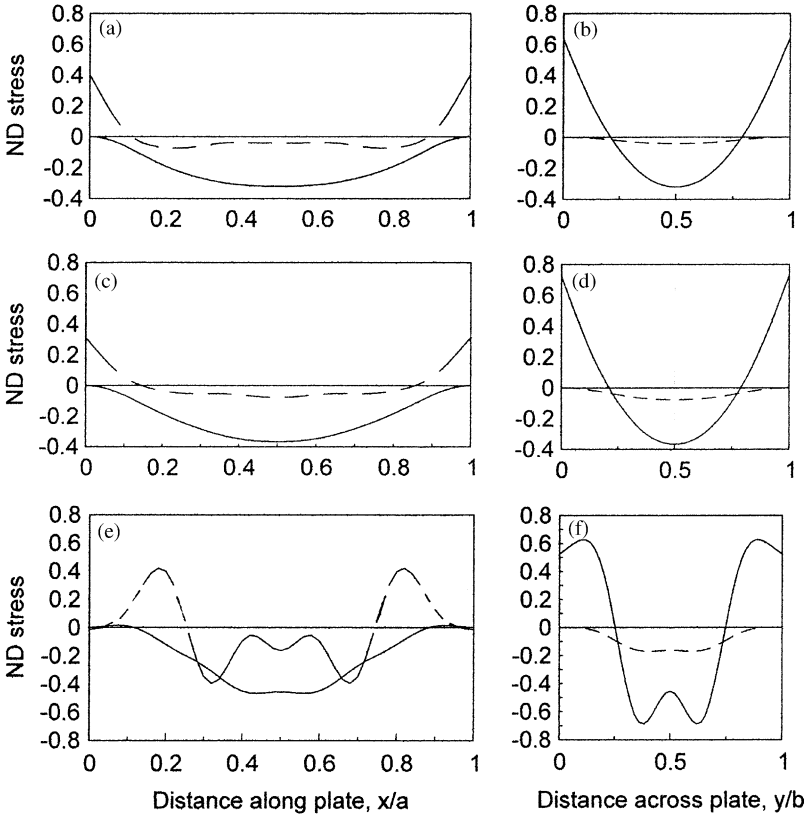

Fig. 3. Variation of the direct stresses along and across the plate centrelines, as generated by the three different temperature distributions. Plate aspect ratio = 2: (a) and (b) distribution (1); (c) and (d) distribution (2); (e) and (f) distribution (3). ————, σ_x; – – – – – –, σ_y.

is due to the differences in the second derivatives of the temperature distributions. For distribution (3) these derivatives are zero over the whole plate except along the lines of temperature discontinuity along which they can be said to be infinite over an infinitesimal distance.[1] Significantly, the stress peaks and troughs and the very rapid stress changes seen in Figs. 3(e) and (f) occur in regions close to the temperature discontinuities.

The average x-wise direct stress over the heated region is significantly greater for distribution (3) than for (1) and (2). Calculations have also been performed for other uniform distributions over both larger and smaller regions than that of (3). They show that the average central stress level is highest (and little different from that of (3)) when the heated region extends from about $x \approx 0.3a$ to $0.7a, y \approx 0.3b$ to $0.7b$. Over a larger region it drops and when the whole plate is uniformly heated, the thermal stress is necessarily zero. Over a smaller region it increases and locally approaches infinity as the region diminishes to zero. It will be seen later that these are

[1] In spite of this, the terms in the right-hand elements of Eq. (5) which involve these derivatives can easily be integrated exactly by parts.

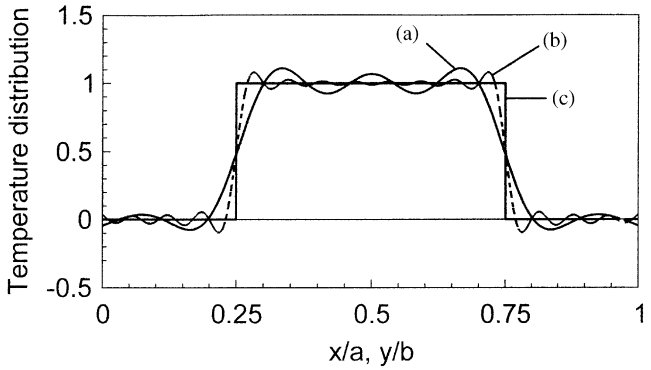

Fig. 4. Reconstructed temperature distributions from the truncated series representing the step-function distribution (3): (a) from the six-term series, (b) from a 14 term series and (c) the step function itself.

crucially important features which govern the critical buckling temperatures of the plate and its frequency–temperature relationships.

Now the method of analysis leading to Eq. (5) effectively represents the second derivative of each temperature distribution by the truncated generalized Fourier series of beam functions. Discontinuous distributions such as (3) are usually poorly represented by such series. The inverse transform of the series can be integrated twice to yield a "reconstructed" temperature distribution to which the computed stresses of Figs. 3(e) and (f) correspond exactly, so they only correspond approximately to the true step-function. Fig. 4 shows two such reconstructions, one from the series with the six symmetrical terms which was actually used and the other from a series of 14 symmetrical terms. The reconstructed distribution (a) is more realistic physically than the "ideal" double step function of distribution (3). Its maximum second derivatives close to the steps are finite, thus generating smaller stresses than would the infinite second derivatives of the ideal step function. A similar reconstruction of the temperature distribution for the parabolic distribution shows that the reconstructed distribution from the six-term series lies within 0.1% of the correct parabolic distribution over the central (and most important) 90% of the span.

3. The flexural modes, frequencies and critical temperatures of a flat free–free plate with in-plane thermal stresses

3.1. Derivation of the equations

The plate now deforms with the transverse displacement $w(x, y, t)$. The modes and frequencies of free vibration can be found by a conventional minimized energy analysis based on expressions for the potential and kinetic energies of the plate. The potential energy derives from the strain energy of flexure (U_{flex}) and work done by the internal stresses as the plate effectively shortens

(U_σ). The expressions for these are well known (e.g., see Ref. [20]):

$$U_{flex} = \frac{D}{2}\int\int\left\{\left[\frac{\partial^2 w}{\partial x^2}+\frac{\partial^2 w}{\partial y^2}\right]^2 - 2(1-\nu)\left[\frac{\partial^2 w}{\partial x^2}\frac{\partial^2 w}{\partial y^2} - \left[\frac{\partial^2 w}{\partial x \partial y}\right]^2\right]\right\} \mathrm{d}x\,\mathrm{d}y, \tag{7}$$

$$U_\sigma = \frac{h}{2}\int\int\left[\sigma_x\left(\frac{\partial w}{\partial x}\right)^2 + 2\sigma_{xy}\left(\frac{\partial w}{\partial x}\frac{\partial w}{\partial y}\right) + \sigma_y\left(\frac{\partial w}{\partial y}\right)^2\right] \mathrm{d}x\,\mathrm{d}y, \tag{8}$$

in which $D = Eh^3/12(1-\nu^2)$ is the plate flexural rigidity and the double integrals are evaluated over the whole plate surface.

With the density of the plate material denoted by ρ, the kinetic energy function is given by

$$T = \frac{\rho h}{2}\int\int\left(\frac{\partial w}{\partial t}\right)^2 \mathrm{d}x\,\mathrm{d}y. \tag{9}$$

$w(x,y)$ is to be expressed in the double series form

$$w(x,y) = \sum_{j=1}^{J}\sum_{k=1}^{K} W_{jk}(t)\phi_j(x)\psi_k(y). \tag{10}$$

Following Lemke [21], Warburton [22,23] and authors already cited [5,6,12], we shall use the beam functions for a free–free beam $\phi_j(x)$, $\psi_k(y)$ together with rigid-body translational and rotational modes. Although the second and third derivatives of these modes vanish at $x = 0, a$ and $y = 0, b$ the product modes in Eq. (10) do not each satisfy the natural boundary conditions at the free edges of the plate. This, of course, is not a necessary requirement in an energy analysis but the modes do usefully satisfy the conditions for zero total transverse and angular momentum of the free–free plate.

A conventional Rayleigh–Ritz or Lagrange equation method leads to the linear matrix equation for the frequency Ω and the generalized co-ordinates $W_{j,k}$ in the form

$$[\bar{\mathbf{K}}_{el} - T_{ND}\bar{\mathbf{K}}_{th} - \Omega^2\bar{\mathbf{M}}]\{\mathbf{W}_{jk}\} = 0, \tag{11}$$

in which $\bar{\mathbf{K}}_{el}$, $\bar{\mathbf{K}}_{th}$ and $\bar{\mathbf{M}}$ are square non-dimensional matrices of order $(J \times K)$, $(J \times K)$. $\bar{\mathbf{K}}_{el}$ is a non-dimensional elastic stiffness matrix derived from U_{flex}. $\bar{\mathbf{K}}_{th}$ is a non-dimensional thermal stiffness matrix derived from U_σ. $\bar{\mathbf{M}}$ is the non-dimensional mass matrix and, by virtue of the orthogonal properties of the ϕ's and ψ's, is diagonal. T_{ND} and Ω are the non-dimensional temperature and frequency, respectively. Appendix B defines and derives these terms and matrices.

The solution of Eq. (11) for the natural frequencies Ω is a standard eigenvalue problem, given the ND temperature T_{ND}. Alternatively, for a given value of Ω it can be solved as an eigenvalue problem for T_{ND}. When Ω is set to zero, the corresponding values of T_{ND} are the (eigenvalue) critical buckling temperatures which create conditions of neutral static stability of the plate.

4. Computed frequencies, modes and critical temperatures

Natural frequencies, modes and critical temperatures have been calculated for a free–free plate of aspect ratio $AR = 2$ and the Poisson ratio $v = 0.3$, free along all four edges and subjected in turn to the three distributions already described. Limited calculations have also been performed for a plate of aspect ratio $AR = 1$, the Poisson ratio $v = 0.3$ and with stress distribution (1).

The plate deflections were described by the first six symmetric and/or antisymmetric beam functions in each plate direction, together with the appropriate rigid body modes, i.e., $(6 + 1)^2 = 49$ different independent product modes were used and 49 eigenvalues were found at a time. The symmetric or antisymmetric modes in the x direction were paired, in turn, with symmetric or antisymmetric modes in the y direction. It can easily be proved [24] that the vibration modes of an unheated plate with general boundary conditions (i.e., with no in-plane stresses) become coupled when a general non-uniform in-plane stress system exists. For this reason, the modes change with changing temperature. However, when the stress distributions are doubly symmetric (as in this paper) they cannot cause coupling between the doubly symmetric modes and the doubly antisymmetric mode. Modes which can be coupled are those which have the same "order of symmetry", i.e., they are both symmetric (or antisymmetric) in one direction, and are both symmetric (or antisymmetric) in the other direction. This condition for no coupling justifies the reduction of the order of the problem in our case to $7 \times 7 = 49$. Otherwise 15 modes would have to be used in each plate direction at a time, leading to an eigenvalue problem of order $15 \times 15 = 225$.

4.1. The buckling temperatures

Table 1 shows some computed critical temperatures for the plate with $AR = 2$ and subjected to the three temperature distributions in turn. That the magnitudes of the positive values are all greater than their negative counterparts is simply explained. Positive temperatures cause the central region of the plate to be compressed and the edges of the plate to be stretched. At a positive critical temperature the central region of the plate buckles, while the surrounding stretched edges exert a stabilizing influence all around it. Negative critical temperatures compress the edges of the plate and stretch the central region so the edge regions buckle, while the central stretched region provides the stabilizing influence. The plate edges are unconstrained so the compressed edge regions are effectively less constrained by plate tension than is the central region

Table 1
Some ND critical temperatures which produce plate buckling

Temperature distribution number	ND critical temperature, T_{ND}			
1	−351.59	−152.92	230.46	557.51
2	−347.4	−141.99	209.25	550.32
3	−319.45	−104.92	139.05	413.69

Free–free plate of aspect ratio $AR = 2$

when that is compressed. The negative buckling temperatures are therefore lower in absolute value than their positive counterparts.

The critical temperatures corresponding to distributions (1) and (2) are similar in magnitude, those of distribution (2) being slightly less than those of (1). This is due simply to the stress levels of (2) for a given temperature being slighter greater than those of (1) as already observed. The critical temperatures corresponding to distribution (3) are smaller than those of (1) and (2) because (as already seen) the stress levels over the central region for a given temperature are greater than those of distributions (1) and (2).

As the uniformly heated region of the plate extends over much more than the central half, the thermal stresses drop and a higher temperature is required to cause buckling. If it extends over a very small central region, the domain in which the stresses are very large is too small for the stresses to have much effect on the low order buckling modes. A higher temperature is required again to cause buckling. Hence, in both of these extreme cases the critical temperatures approach infinity.

Table 2 shows how the computed critical temperatures for distribution (2) converge as the number of modes used in the calculation is increased from two elastic modes + one rigid-body mode in each plate direction (3^2 modes in all) to six elastic modes + one rigid-body mode (7^2 modes in all). For the six sets shown, the 49-mode results have evidently converged satisfactorily.

It is pertinent to consider the actual temperatures required to cause buckling in a plate of given material and size, rather than the non-dimensional (ND) values. Consider an aluminium plate 1 m long, 0.5 m wide, 1 mm thick, with Young's modulus $E = 70$ G N/m^2 and linear expansion coefficient $\alpha = 2.3 \times 10^{-5}$. The lowest ND positive critical temperature for distribution (2) is 209.25, which corresponds in this case to an actual temperature of only 1.67°C (from Eq. (B.10)). The maximum x-wise compressive stress generated by this occurs at the plate centre and is $0.38ET_0\alpha = 1.019$ N/mm^2 (see Fig. 3(c) for the 0.38 factor).

At first sight this appears to be very low but one can show at least that it is of the right order of magnitude by comparing it with the buckling stress of a uniformly compressed plate of an equivalent size. An "equivalent size" cannot be precisely defined but the following process can be followed which makes use of Fig. 5. This shows surface and contour plots of the transverse modal deflection of the buckled plate at $T_{ND} = 209.25$. Within the contour $w(x, y) = 0$ the mode is nearly sinusoidal with half-wavelengths in both x and y directions of approximately $0.55a$. Let

Table 2
Convergence of the ND critical temperatures with increasing number of mode combinations used in computation; temperature distribution 2

Number of modes used	ND critical temperatures					
9 (2)	−1089.5	−359.13	−143.56	210.45	601 45	7246.9
16 (3)	−656.73	−349.58	−142.73	209.85	551.64	1303.8
25 (4)	−637.04	−348.39	−142.37	209.53	550.99	1097.9
36 (5)	−634.86	−347.83	−142.14	209.36	550.53	1092.1
49 (6)	−634.3	−347.4	−141.99	209.26	550.32	1091.5

The bracketted number is the number of beam functions used to describe the transverse displacement in either direction.

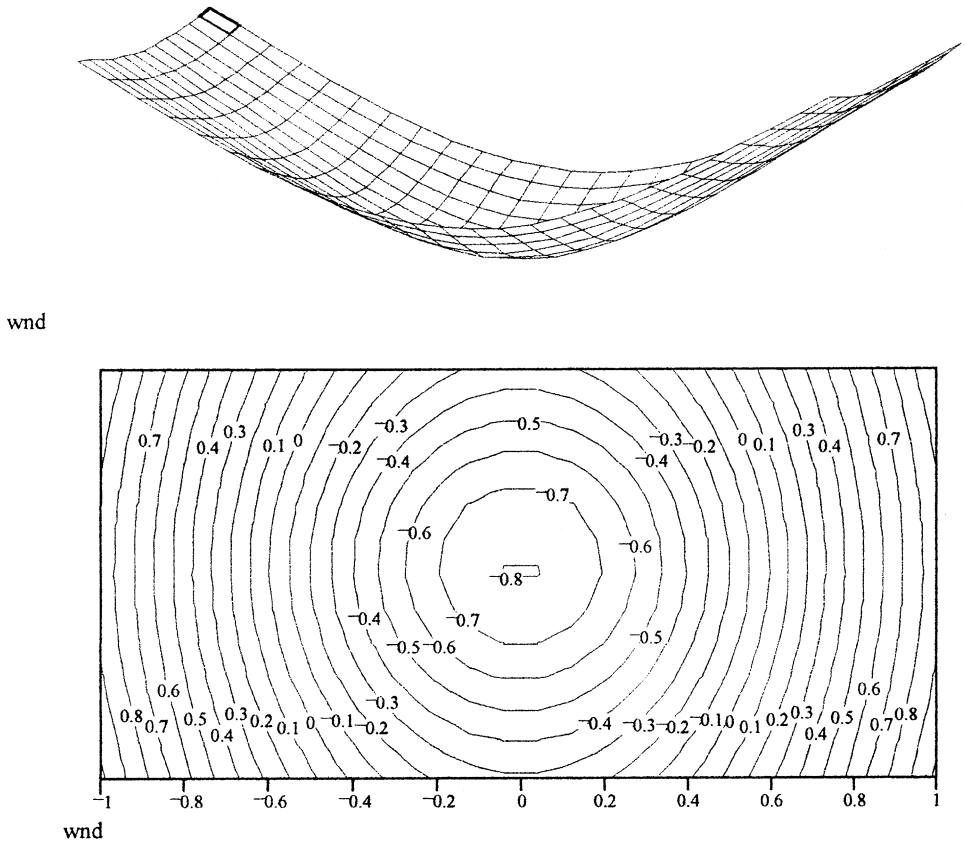

Fig. 5. Surface and contour plots of the transverse mode of plate buckling at $T_{ND} = 209.25$; temperature distribution (2). Plate aspect ratio = 2.

these half-wavelengths be the length and breadth, a_e and b_e, of the "equivalent" simply supported rectangular plate. Under uniform compression in both directions its x-wise buckling stress is given by $\sigma_x = (\pi^2 D/(a^2 b^2 h))(a^3 + b^{2/})^3/(b^2 + (\sigma_y/\sigma_x)a^2)$ (see Ref. [20]). In the present case $\sigma_y \approx 0.2\sigma_x$ at the centre of the plate (see Figs. 3(c) and (d)). With $a_e = b_e = 0.55$ the x-wise buckling stress is found to be 0.70 N/mm^2 which is well within an order of magnitude of the value of 1.019 N/mm^2 already quoted for the actual thermally stressed plate. Closer agreement would not be expected with such a crude equivalent model.

4.2. Natural frequencies and modes

ND frequencies Ω have been found in the standard way as the eigenvalue solutions of Eq. (11) (see also Eq. (B.9) of Appendix B). To check the correctness of the computed mass and elastic stiffness matrices, frequencies were first found for a square plate ($AR = 1.0$) with the Poisson ratio $\nu = 0.3$ and with no thermal stresses ($T_{ND} = 0$). The two lowest ND values so found are compared in Table 3 with values obtained in previous work, the close agreement confirming the correctness

Table 3
ND natural frequencies of a square free–free plate as computed by various authors

Mode no.	Leissa [25]	Iguchi [26]	Bardell [27]	Present work
4	13.489	13.473	13.468	13.475
5	19.789	19.596	19.596	19.671
6	24.432	24.27	24.27	24.337
7	35.024	34.801	34.801	34.897

The Poisson ratio $v = 0.3$.

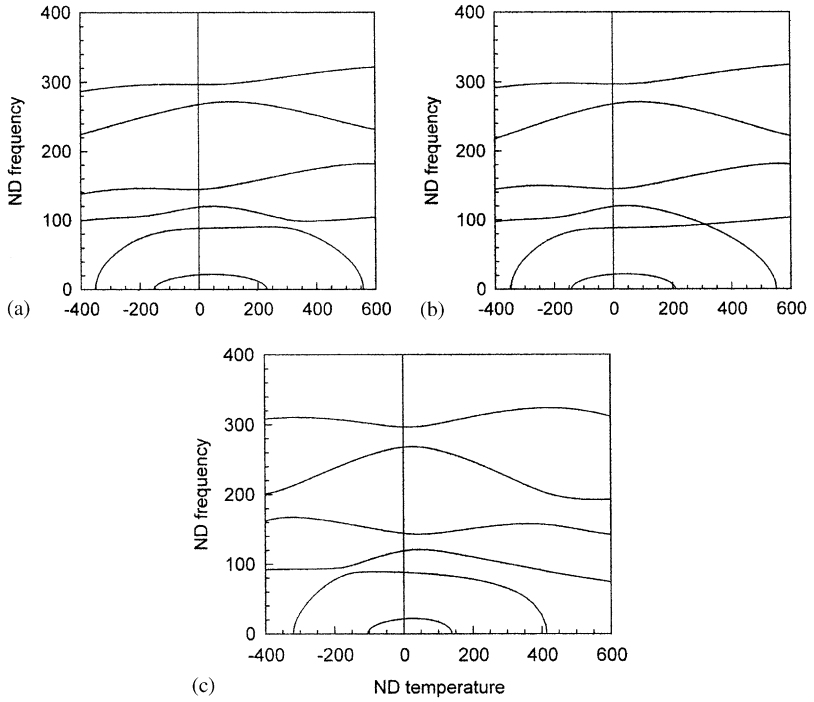

Fig. 6. The variation with temperature T_{ND} of the ND frequency Ω of the plate of Fig. 3. Plate aspect ratio = 2, the Poisson ratio = 0.3: (a) temperature distribution (1), (b) distribution (2), and (c) distribution (3).

of the matrices of the present work. The mode numbering in the table excludes modes 1–3 which are rigid-body zero-frequency modes. Modes 4 and 5 are doubly symmetric, mode 6 is doubly antisymmetric (a torsional mode) and mode 7 is symmetric in one direction and antisymmetric in the other.

Figs. 6(a)–(c) show the variation with ND temperature of the frequencies of the doubly symmetric modes of the free–free plate of aspect ratio $AR = 2$, subjected in turn to the three different temperature distributions. Each figure shows that a progressive rise or fall of the temperature eventually causes the frequency of first one mode and then the next to drop to zero at

the critical buckling temperatures of the plate. It is recognized that the only temperature range of practical significance is on either side of $T_{ND} = 0$ between the pair of nearest buckling temperatures. Outside this range, the plate is statically unstable and even before these limits are reached large static plate deflections will occur if it is not initially perfectly flat. In turn, these deflections modify the stress distributions and complicate the whole analysis. The analysis presented in this paper, of course, is entirely linear and assumes perfect initial flatness of the plate.

Fig. 6 shows that a small increase of temperature from $T_{ND} = 0$ increases the frequencies of some modes (albeit slightly) but decreases the frequencies of others. The same phenomenon was observed by Bailey [12] in his plate studies and by Mead [3] in his study of thermally strained beam and frame systems. This asymmetry of the frequency versus temperature curves about $T_{ND} = 0$ is due entirely to the differences in the magnitudes of the positive and negative critical temperatures, this difference being due in turn to the different modes of thermal buckling at those temperatures. However, even at low levels of non-uniform temperature, the internal thermal stresses change the effective flexural stiffness of different parts of the plate and this, of course, must influence the natural frequencies. Compressive thermal stress in the central region of the plate effectively reduces the local flexural stiffness while the simultaneous tensile stress in the edge regions effectively increases the local flexural stiffness. Large enough compressive stresses lead to buckling of the central region and the vanishing of a frequency.

Evidence of these effects on the local flexural stiffness can be seen in Fig. 7 which shows the first two normalized doubly symmetric modes of the plate with $AR = 2$ under temperature distribution

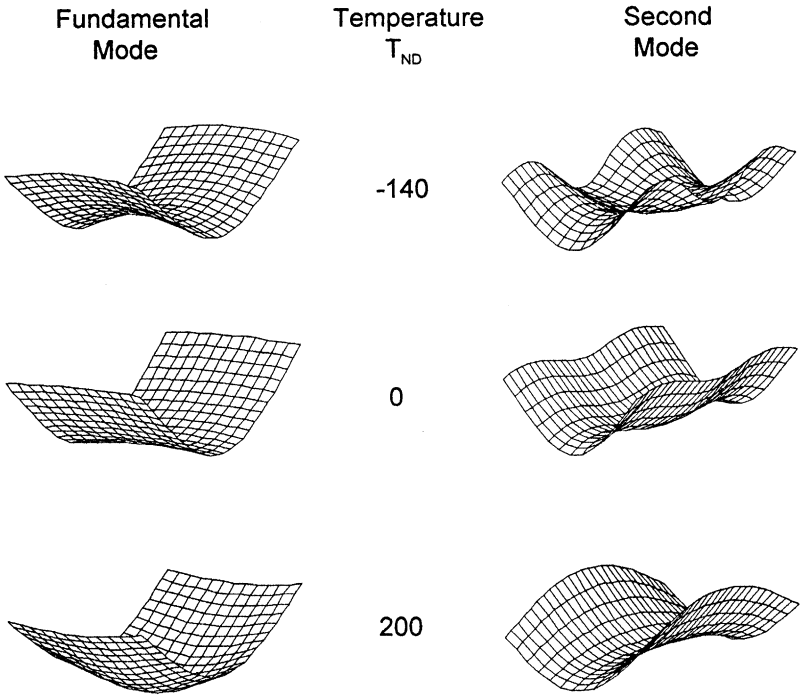

Fig. 7. Modes of vibration corresponding to the frequencies of Fig. 6(b) at three different temperatures. Plate aspect ratio, $AR = 2.0$, the Poisson ratio, $\nu = 0.3$.

(2) at the ND temperatures of $T_{ND} = -140, 0, +200$. Detailed examination shows the central regions of the plate to have higher relative curvatures and deflections when the central stress is compressive ($T_{ND} = 200$) than when it is tensile ($T_{ND} = -140$) simply because the local flexural stiffness is reduced by compression. The edge regions of the plate have higher curvatures and deflections when the edge stress is compressive ($T_{ND} = -140$) than when it is tensile. The changes in the modal curvatures of the fundamental modes are not very pronounced but are quite dramatic for the second and higher modes. Fig. 7 also shows the very significant mode change as the temperature changes. This violates the basic assumption underlying the linear law relating Ω^2 and T_{ND} so the linear law cannot be applicable in this case.

The frequencies of modes which have antisymmetric deflections in one or both directions are shown in Fig. 8 for the plate with $AR = 2$ and temperature distribution (1). Fig. 8(a) relates to the doubly antisymmetric modes, Fig. 8(b) to the y-wise antisymmetric and x-wise symmetric modes and Fig. 8(c) to the x-wise antisymmetric and y-wise symmetric modes. Over the indicated temperature range, modes which have y-wise antisymmetric deflections (Figs. 8(a) and (c)) have no positive critical temperatures in the indicated range and the frequencies continue to rise with increasing T_{ND}. However, further calculations show that positive critical temperatures exist at much higher values, e.g., $T_{ND} = 2244$ for the lowest curve of Fig. 8(a) and $T_{ND} = 2090$ for the lowest curve of Fig. 8(c). These critical temperatures, of course, take the plate far outside its statically stable state and are therefore only of academic interest. Their existence, however, contributes to an understanding of the nature of the curves in the realistic T_{ND} region of the curves, as will be seen later.

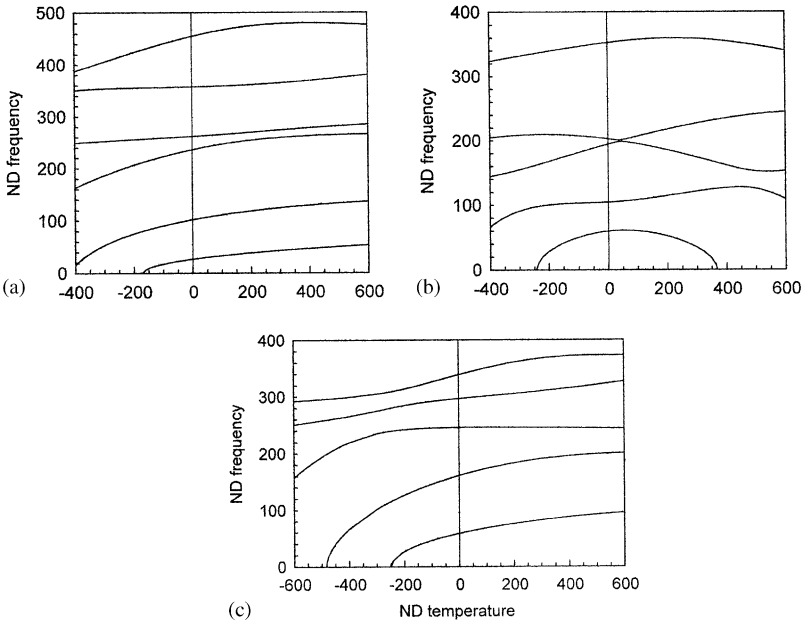

Fig. 8. Comparison of frequencies of doubly symmetric modes with modes having antisymmetric deflections. $AR = 2$, $\nu = 0.3$, temperature distribution (1): (a) doubly antisymmetric modes, (b) y-wise antisymmetric with x-wise symmetric modes, and (c) x-wise antisymmetric with y-wise symmetric modes.

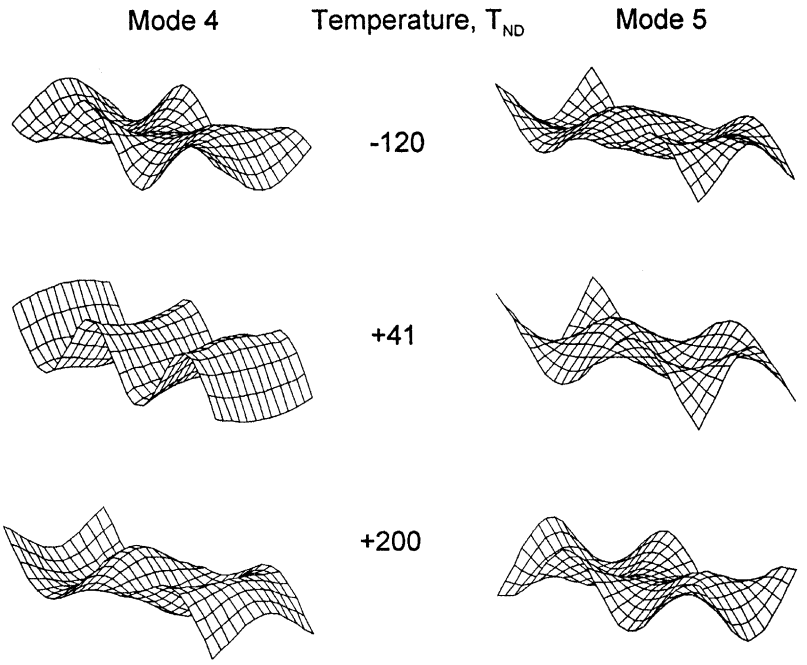

Fig. 9. Modal interchange illustrated by the modes for the second and third curves of Fig. 6(b) at three different ND temperatures.

When the modes are x-wise antisymmetric and y-wise symmetric (Fig. 8(b)) the curves behave in a similar way to those for doubly symmetric modes (Figs. 6(a)–(c)) over the indicated T_{ND} range. The distinguishing feature, however, is the apparent crossing of the curves for modes 3 and 4 at a temperature within the statically stable temperature range of the plate. Detailed numerical examination shows that the curves do not actually cross but approach one another to within $\Delta\Omega/\Omega = 1.2\%$ and then veer away. The mode corresponding to one curve changes dramatically as the curve approaches the other, the modes eventually interchanging their forms. Fig. 9 shows the modes corresponding to the third and fourth curves of Fig. 8(c) at the almost equi-spaced T_{ND} values of -120, $+41$, $+200$. The modes are numbered 4 and 5 in Fig. 9 as mode 1 is the zero-frequency rigid-body rotational mode.

4.3. The limited validity of the linear relationship between Ω^2 and T_{ND}

As stated in the Introduction, the relationship between ω^2 (or Ω^2) and the temperature is linear provided the natural modes of vibration in the absence of in-plane stress are exactly the same as the buckling modes of the plate under the applied in-plane stress system. Fig. 7 has shown conclusively that this is not so for a free–free plate under the temperature distribution (2). ($T_{ND} = -140$ and 200 in Fig. 7 are very close to the buckling temperatures, so the corresponding fundamental modes are almost the same as the buckling modes.)

Figs. 10(a) and (b) show Ω^2 versus T_{ND} for the three lowest order doubly symmetric modes and the three lowest order doubly antisymmetric modes of the plate of aspect ratio 2.0 under

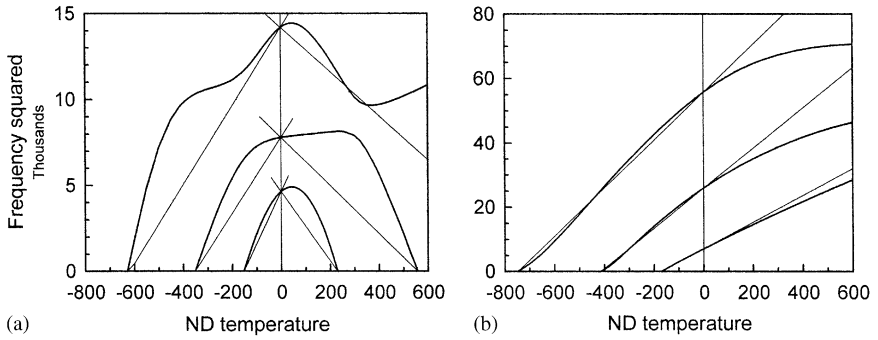

Fig. 10. Ω^2 versus T_{ND} for the plate of aspect ratio $AR = 2$ with non-uniform temperature distribution (1); comparison with linear approximations: (a) for doubly symmetric modes and (b) for doubly antisymmetric modes.

temperature distribution (1). The ordinates of the lower curves on each figure have been multiplied by appropriate factors (as indicated on the figure captions) to present them all clearly on the same vertical scale. The inclined straight lines on these figures represent the simple linear Ω^2 versus T_{ND} relationship and are multiplied by the same factors. These lines join each Ω^2 at $T_{ND} = 0$ with $\Omega^2 = 0$ at the appropriate critical temperatures.

The linear relationship is clearly inapplicable for the doubly symmetric modes for the reason already stated. It does, however, appear to be a good approximation for the doubly antisymmetric modes over the negative temperature range (when the edges of the plate are in compression) and also well into the positive temperature range. At much higher positive ND temperatures, the frequencies of these antisymmetric modes drop in the same way as those of the doubly symmetric modes. They eventually vanish at the critical temperatures $T_{ND} = 2244$, 2877, 3824 for the three curves shown and this leads to the eventual breakdown of the linear Ω^2 versus T_{ND} relationship.

Detailed examination of any Ω^2 versus T_{ND} curve close to a critical temperature (positive or negative) shows it to lie very close to and wavering around the line of a linear Ω^2 versus T_{ND} relationship, but this straight line does not in general pass through the correct zero-temperature frequency. The magnitude of the discrepancy depends entirely on the relative magnitudes of the positive and negative critical temperatures of the actual curve. If the positive critical temperature, $T_{NDcrit,+}$ is an order of magnitude greater than its negative counterpart, $T_{NDcrit,-}$ (i.e., $T_{NDcrit,+} \gg |T_{NDcrit,-}|$) the discrepancy is small over the temperature range $T_{crit,-} < T_{ND} < 0$. This condition is satisfied by the modes and frequencies of Fig. 10(b). It is not satisfied by those of Figs. 10(a) and 7(b),(c). For all of the modes and frequencies of these figures $|T_{NDcrit,-}|$ is less than $T_{crit,+}$ but their ratios are not sufficiently great.

The square plate ($AR = 1$) displays some unique features. Fig. 11 shows Ω and Ω^2 versus T_{ND} curves for the plate under temperature distribution (1). Figs. 11(a) and (b) cover limited temperature ranges while Fig. 11(c) covers a much extended (albeit unrealistic) range. The Ω versus T_{ND} curves are broadly similar to those for the plate with $AR = 2$ (Fig. 6(a)) except that the bottom two curves for the square plate actually cross in the temperature range of static stability. At the crossing point two modes exist with identical frequencies, i.e., classically degenerate modes. The sixth and seventh curves also cross within the same temperature range.

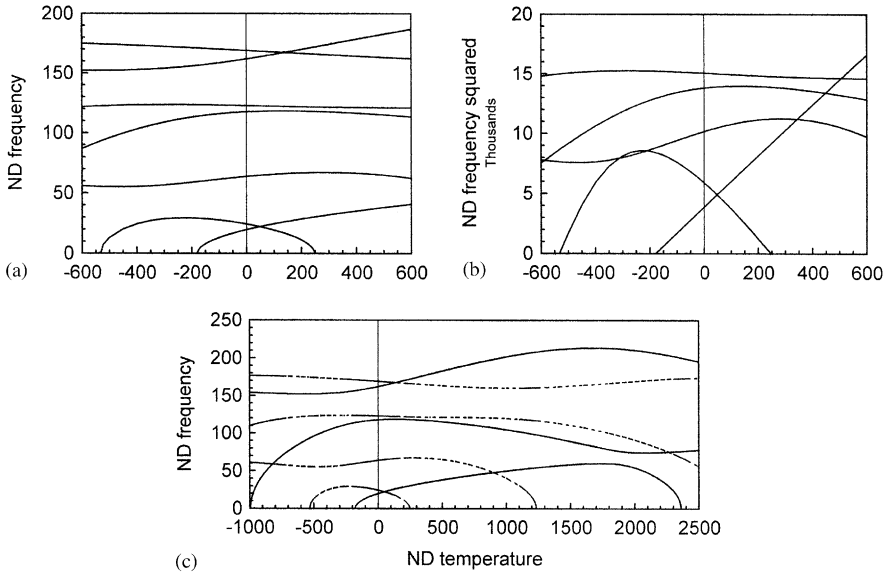

Fig. 11. Ω versus T_{ND} and Ω^2 versus T_{ND} for the for doubly symmetric modes of the plate with $AR = 1$ and non-uniform temperature distribution (1): (a) Ω versus T_{ND}, (b) Ω versus T_{ND} and (c) Ω versus T_{ND}, extended temperature range. The ordinates of the two lowest curves of (b) have been factored by 10 and those of the third lowest by 2.5.

This contrasts with the plate with $AR = 2$ (Fig. 10) the curves of which only approach one another and then veer away. It is well known that unstressed square plates can have different modes with identical frequencies, but not when the associated modes are both doubly symmetric or doubly antisymmetric.

The curves of Ω^2 for the square plate[2] (Fig. 11(b)) are significantly different from those of the rectangular plate (Fig. 10(a)). Notice that the curve for the lowest order square plate is as straight (i.e., linear) as the eye can see between the pair of critical temperatures closest to $T_{ND} = 0$. This appears to violate the criterion stated above that $T_{NDcrit,+}$ should be much greater than $|T_{NDcrit,-}|$ for Ω^2 linearity to occur over such a wide range. In fact, this criterion *is* satisfied in the present case and is demonstrated by Fig. 11(c). This shows that the positive T_{NDcrit} corresponding to $T_{NDcrit} = -175$ (at which the straight inclined line begins) is *not* the T_{NDcrit} of $+247$ in the figure. $T_{NDcrit} = +225$ belongs to the curve which starts at $T_{NDcrit} = -529$. The curve starting at $T_{NDcrit} = -175$ crosses this curve, goes on rising, crossing yet another curve which joins $T_{NDcrit} = -1000$ and $+1230$ before dropping to its own positive $T_{NDcrit,+}$ of $+2362$. This critical temperature is very much greater than its negative counterpart of -175, so together they amply satisfy the high ratio criterion for a wide range of linear Ω^2. Examination of the vibration modes along the curve from $T_{ND} = -175$ to $+2362$ shows them to remain remarkably constant up to about $T_{ND} = +1500$. Thereafter they begin to change and become quite different at $T_{ND} = +2362$.

[2] Each curve of Fig. 11b has been multiplied by a different factor in the same way as the curves of Figs. 10(a) and (b).

Notice also that the Ω^2 curve in Fig. 11(b) joining $T_{NDcrit} = -532$ and $T_{NDcrit} = +247$ is hardly straight at all over its whole temperature range. Its T_{NDcrit} ratio is only 0.46 so the high ratio criterion is not satisfied and the linear Ω^2 versus T_{ND}. relationship is quite inapplicable.

5. Conclusions

The natural frequencies and flexural modes of a flat unsupported plate can be dramatically changed by the in-plane stresses induced by non-uniform thermal strains. A Rayleigh–Ritz method which incorporates the associated in-plane potential energy terms is suitable for finding the frequencies and modes of such plates.

The different non-uniform surface temperature distributions considered in this paper, all doubly symmetric with respect to the plate centrelines, cause the frequencies of the fundamental doubly symmetric and antisymmetric modes initially to rise as the temperature at the plate centre rises above that of the edges. Thereafter they level off before dropping to zero at a different positive critical (buckling) temperature for each type of mode. This temperature can be very high for antisymmetric modes. When the plate centre temperature drops below that of the edges, the fundamental frequencies drop and eventually vanish at negative critical temperatures which differ from the positive values. The effect of temperature on higher mode frequencies is variable, some rising, some falling as the temperature rises from zero. All drop to zero at high order positive and negative critical temperatures. The magnitudes of the critical temperatures depend, amongst other factors, on the temperature distribution function, in particular on its second space derivatives.

For a free plate of aspect ratio 2, the so-called "linear law" for the relationship between the square of the frequency and the temperature does not apply to its doubly symmetric modes due to the considerable change in the mode as the temperature changes. Some modes change dramatically between their critical temperatures, the ratio of which determines the rate of mode change. For some of the antisymmetric modes this ratio is high and the rate of mode change is low over a large part of the temperature range over which the actual frequency follows the linear law quite closely.

The square plate displays unique features. At certain temperatures, degenerate modes with identical frequencies can exist of the same symmetry class, i.e., both modes can be doubly symmetric or both can be antisymmetric. Moreover, the frequency of the fundamental doubly symmetric mode of the square plate can be well approximated by the linear law.

When the plate centre is heated relative to its edges, the central region is compressed and its modal curvatures and deflections tend to increase. When the plate centre is cooled (edges hotter than the centre) the edges are compressed and their curvatures and deflections tend to increase. Understanding such features assists in explaining the different magnitudes of the positive and negative critical temperatures. Plate edges compressed due to a negative central temperature are much more susceptible to buckling than the central region of the plate when compressed due to a positive temperature. The absolute value of the negative critical temperature of a free plate is therefore smaller than the corresponding positive critical temperature. As a result, the fundamental frequency initially rises as the temperature rises from zero.

Appendix A. The matrix equation for the thermal stress function

Introduce the following non-dimensional variables into the bi-harmonic equation for ϕ: $\xi = x/a$, $\eta = y/b$, $T = T_0 t(\xi,\eta)$ and AR (the plate aspect ratio) $= a/b$. The equation becomes

$$\frac{1}{AR^2}\frac{\partial^4\phi}{\partial\xi^4} + 2\frac{\partial^4\phi}{\partial\xi^2\partial\eta^2} + AR^2\frac{\partial^4\phi}{\partial\eta^4} = -E\alpha T_0 ab\left\{\frac{1}{AR}\frac{\partial^2 t}{\partial\xi^2} + AR\frac{\partial^2 t}{\partial\eta^2}\right\}. \tag{A.1}$$

Solutions for $\phi(\xi,\eta)$ are sought in the double series form:

$$\phi(\xi,\eta) = \sum_{m=1}^{M}\sum_{n=1}^{N} A_{mn} f_m(\xi) g_n(\eta), \tag{A.2}$$

where $f_m(\xi), g_n(\eta)$ are the beam functions for a vibrating uniform beam clamped at each end and have the familiar form [28]

$$f_m(\xi) = \cosh\lambda_m\xi - \cos\lambda_m x - \sigma_m(\sinh\lambda_m\xi - \sin\lambda_m\xi), \tag{A.3}$$

where

$$\sigma_m = \frac{(\cosh\lambda_m - \cosh\lambda_m)}{(\sinh\lambda_m - \sin\lambda_m)} \tag{A.4}$$

The function $g_n(\eta)$ has precisely the same form as $f_m(\xi)$ but with η $(= y/b)$ replacing ξ. For the first three functions $\lambda_1 = 4.7300407449$, $\lambda_2 = 7.88532046241$, $\lambda_3 = 10.995607838$. The λ_m's for higher m values are listed in Ref. [28] and in many other standard texts.

Numerical calculations based on this particular form of $f_m(\xi)$ can become ill-conditioned at high values of m when the two hyperbolic terms become extremely large and almost equal. The problem is circumvented by expressing $f_m(\xi)$ in the alternative form

$$f_m(\xi) = \exp(-\lambda_m\xi) - \cos\lambda_m\xi - \delta_m\sinh\lambda_m\xi + \sigma_m\sin\lambda_m\xi, \tag{A.5}$$

where

$$\delta_m = 2\left[\frac{\exp(-2\lambda_m) + [\sin\lambda_m - \cos\lambda_m]\exp(-\lambda_m)}{1 - \exp(-2\lambda_m) - 2\exp(-\lambda_m)\sin\lambda_m}\right]. \tag{A.6}$$

The A_{mn}'s for a given temperature distribution $t(\xi,\eta)$ can be found from the set of linear equations formed by multiplying both sides of Eq. (A.1) by each product $f_r(\xi)g_s(\eta)$ in turn ($r = 1$–$M, s = 1$–N) and then by integrating both sides of the equation over the whole plate surface. In this process the double (surface) integrals become products of single integrals, many of which vanish by virtue of the orthogonal property of the $f(\xi)$'s and $g(\eta)$'s. The whole process yields the matrix equation (see Eq. (5) in the main text)

$$[\mathbf{C}]\{\mathbf{A}_{mn}\} = -E\alpha ab T_0\{\mathbf{RHS}\}, \tag{A.7}$$

where [**C**] is of order $(M \times N)$, $(M \times N)$. Its general off-diagonal term is

$$C_{rs,mn} = 2\int_0^1 f_r(\xi) f_m''(\xi)\,\mathrm{d}\xi \int_0^1 g_s(\eta) g_n''(\eta)\,\mathrm{d}\eta.$$

Since the chosen f and g functions are of identical form, this is the same as $2\int_0^1 f_r(\xi)f_m''(\xi)\,\mathrm{d}\xi \int_0^1 f_s(\xi)f_n''(\xi)\,\mathrm{d}\xi$. Moreover, the beam functions of the clamped beam have the

further property $\int_0^1 f_r(\xi)f_m''(\xi)\,\mathrm{d}\xi = \int_0^1 f_m(\xi)f_r''(\xi)\,\mathrm{d}\xi = -\int_0^1 f_r'(\xi)f_m'(\xi)\mathrm{d}\xi$ so the general off-diagonal term has the alternative form

$$C_{rs,mn} = 2\int_0^1 f_r'(\xi)f_m'(\xi)\,\mathrm{d}\xi \int_0^1 f_s'(\xi)f_n'(\xi)\,\mathrm{d}\xi \quad (rs \neq mn). \tag{A.8}$$

The diagonal elements of the **C** matrix are identified by $r = m,\ s = n$ and its elements are found to be

$$C_{mn,mn} = 2\int_0^1 [f_m'(\xi)]^2\,\mathrm{d}\xi \int_0^1 [f_n'(\xi)]^2\,\mathrm{d}\xi + \frac{1}{AR^2}\lambda_m^4 \int_0^1 f_m^2(\xi)\,\mathrm{d}\xi \int_0^1 g_n^2(\eta)\,\mathrm{d}\eta + AR^2\lambda_n^4 \int_0^1 f_m^2(\xi)\,\mathrm{d}\xi \int_0^1 g_n^2(\eta)\,\mathrm{d}\eta.$$

For the particular functions chosen $\int_0^1 f_m^2(\xi)\,\mathrm{d}\xi = \int_0^1 g_n^2(\eta)\,\mathrm{d}\eta = 1$ for all values of m and n so the general diagonal term of **C** becomes

$$C_{mn,mn} = 2\int_0^1 [f_m'(\xi)]^2\,\mathrm{d}\xi \int_0^1 [f_n'(\xi)]^2\,\mathrm{d}\xi + \frac{\lambda_m^4}{AR^2} + AR^2\lambda_n^4. \tag{A.9}$$

The terms of the right side of Eq. (A.7) depend upon the temperature distribution function $t(\xi,\eta)$. When this has a simple two-dimensional parabolic form with its maximum at the plate centre, $t(\xi,\eta) = 16(\xi - \xi^2)(\eta - \eta^2)$ the whole m,n term on the right side is

$$E\alpha T_0 ab\left\{\frac{1}{AR}\int_0^1 8f_m(\xi)\,\mathrm{d}\xi \int_0^1 4g_n(\eta)(\eta - \eta^2)\,\mathrm{d}\eta + AR\int_0^1 8g_n(\eta)\,\mathrm{d}\eta \int_0^1 4f_m(\xi)(\xi - \xi^2)\,\mathrm{d}\xi\right\}.$$

Once again, for the special case under consideration we can express this solely in terms of the f-functions and the ξ co-ordinate as

$$E\alpha T_0 ab\left\{\frac{1}{AR}\int_0^1 8f_m(\xi)\,\mathrm{d}\xi \int_0^1 4f_n(\xi)(\xi - \xi^2)\,\mathrm{d}\xi + AR\int_0^1 8f_n(\xi)\,\mathrm{d}\xi \int_0^1 4f_m(\xi)(\xi - \xi^2)\,\mathrm{d}\xi\right\}. \tag{A.10}$$

Evaluating the terms of Eq. (A.7) one can solve it for unit value of $-E\alpha T_0 ab$. This yields a non-dimensional stress function ϕ_{ND} such that $\phi = -\phi_{ND}E\alpha T_0 ab$. Putting this into the expressions for $\sigma_x, \sigma_y, \tau_{xy}$ and introducing $\xi = x/a,\ \eta = y/b$ one finds

$$\sigma_x = -E\alpha T_0 AR\frac{\partial^2\phi_{ND}}{\partial\eta^2}, \tag{A.10a}$$

$$\sigma_y = -E\alpha T_0\frac{1}{AR}\frac{\partial^2\phi_{ND}}{\partial\xi^2}, \tag{A.10b}$$

$$\tau_{xy} = E\alpha T_0\frac{\partial^2\phi_{ND}}{\partial\xi\partial\eta} \tag{A.10c}$$

Appendix B. The stiffness and mass matrices for the thermally stressed vibrating free–free plate

In terms of the non-dimensional co-ordinates (ξ,η) the elastic potential energy is

$$U_{flex}=\frac{D}{2ab}\int_0^1\int_0^1\left\{\frac{1}{AR^2}\left(\frac{\partial^2 w}{\partial\xi^2}\right)^2+AR^2\left(\frac{\partial^2 w}{\partial\eta^2}\right)^2+2\nu\frac{\partial^2 w}{\partial\xi^2}\frac{\partial^2 w}{\partial\eta^2}+2(1-\nu)\left(\frac{\partial^2 w}{\partial\xi\partial\eta}\right)^2\right\}\mathrm{d}\xi\,\mathrm{d}y, \tag{B.1}$$

in which $w(\xi,\eta)$ is to be expressed in the form

$$w(\xi,\eta)=\sum_{j=1}^{J}\sum_{k=1}^{K}W_{jk}\phi_j(\xi)\psi_k(\eta). \tag{B.2}$$

The elastic stiffness matrix is set up in the usual way by evaluating $\partial U_{flex}/\partial W_{rs}$ ($rs=1$ to $J\times K$) which leads to row rs of this matrix:

$$\begin{aligned}\frac{\partial U_{flex}}{\partial W_{rs}}=\frac{D}{ab}\sum_{jk=1}^{J\times K}W_{jk}\Bigg[&\frac{1}{AR^2}\int_0^1\phi_r''(\xi)\phi_j''(\xi)\,\mathrm{d}\xi\int_0^1\psi_s(\eta)\psi_k(\eta)\,\mathrm{d}\eta\\&+AR^2\int_0^1\phi_r(\xi)\,\phi_j(\xi)\,\mathrm{d}\xi\int_0^1\psi_s''(\eta)\psi_k''(\eta)\,\mathrm{d}\eta\Bigg]\\+\;2\nu\Bigg[&\int_0^1\phi_j''(\xi)\phi_r(\xi)\,\mathrm{d}\xi\int_0^1\psi_k(\eta)\psi_s''(\eta)\,\mathrm{d}\eta\\&+\int_0^1\phi_j(\xi)\,\phi_r''(\xi)\,\mathrm{d}\xi\int_0^1\psi_k''(\eta)\psi_s(\eta)\,\mathrm{d}\eta\Bigg]\\+\;4(1-\nu)\Bigg[&\int_0^1\phi_j'(\xi)\phi_r'(\xi)\,\mathrm{d}\xi\int_0^1\psi_k'(\eta)\psi_s'(\eta)\,\mathrm{d}\eta)\,\mathrm{d}\eta\Bigg].\end{aligned} \tag{B.3}$$

In the off-diagonal elements of the matrix (i.e., $r\neq j,\ s\neq k$) the first two integral products in this expression vanish completely by virtue of the orthogonality of the beam functions. However, $\int_0^1\phi_j(\xi)\phi_r''(\xi)\,\mathrm{d}\xi\neq\int_0^1\phi_r(\xi)\phi_j''(\xi)\,\mathrm{d}\xi\neq\int_0^1\phi_r'(\xi)\phi_j'(\xi)\,\mathrm{d}\xi$ for the free–free beam functions, unless one function is symmetric and the other is antisymmetric in which case they are all zero. This contrasts with the corresponding integrals for the clamped beam functions which do all vanish for $r\neq j,\ s\neq k$.

The thermal stiffness matrix is derived from the expression for the work done by the internal stresses when the plate deflects by $w(x,y)$ (see Eq. (8) in the main text). In terms of non-dimensional co-ordinates this expression becomes

$$U_\sigma=\frac{h}{2}\int_0^1\int_0^1\left[\frac{1}{AR}\sigma_x\left(\frac{\partial w}{\partial\xi}\right)^2+2\sigma_{xy}\left(\frac{\partial w}{\partial\xi}\frac{\partial w}{\partial\eta}\right)+AR\sigma_y\left(\frac{\partial w}{\partial\eta}\right)^2\right]\mathrm{d}\xi\,\mathrm{d}\eta. \tag{B.4}$$

The stresses σ_x, σ_{xy}, σ_y are given by Eq. (A.10a)–(A.10c) and $w(x,y)$ is given again by Eq. (B.2). Substituting these into Eq. (B.4) and differentiating it with respect to W_{rs} yields row rs of the

thermal stiffness matrix:

$$\frac{\partial U_\sigma}{\partial W_{rs}} = -E\alpha T_0 h \sum_{jk=1}^{J\times K} W_{jk} \sum_{mn=1}^{M\times N} A_{mn}\{I_1 - I_2 - I_3 + I_4\}, \tag{B.5}$$

where

$$I_1 = \int_0^1 f_m(\xi)\phi_r'(\xi)\phi_j'(\xi)\,\mathrm{d}\xi \int_0^1 g_n''(\eta)\psi_s(\eta)\psi_k(\eta)\,\mathrm{d}\eta, \tag{B.6a}$$

$$I_2 = \int_0^1 f_m'(\xi)\phi_r'(\xi)\phi_j(\xi)\,\mathrm{d}\xi \int_0^1 g_n'(\eta)\psi_s(\eta)\psi_k'(\eta)\,\mathrm{d}\eta, \tag{B.6b}$$

$$I_3 = \int_0^1 f_m''(\xi)\phi_r(\xi)\phi_j(\xi)\,\mathrm{d}\xi \int_0^1 g_n(\eta)\psi_s'(\eta)\psi_k'(\eta)\,\mathrm{d}\eta, \tag{B.6c}$$

$$I_4 = \int_0^1 f_m''(\xi)\phi_r(\xi)\phi_j(\xi)\,\mathrm{d}\xi \int_0^1 g_n(\eta)\psi_s'(\eta)\psi_k'(\eta)\,\mathrm{d}\eta. \tag{B.6d}$$

The mass matrix for the vibrating plate is diagonal when the prescribed modes are the products of the free–free beam functions. Its familiar general term is

$$M_{mn,mn} = \rho abh \int_0^1 f_m^2(\xi)\,\mathrm{d}\xi \int_0^1 g_n^2(\eta)\,\mathrm{d}\eta, \tag{B.7}$$

in which each integral has unit value when the ortho-normal beam function modes are used.

The elements of each matrix have thus been expressed as products of a dimensional term (the same for each element in a given matrix) times linear functions of non-dimensional integrals. Introducing the non-dimensional matrices $\bar{\mathbf{K}}_{el}$, $\bar{\mathbf{K}}_{th}$ and $\bar{\mathbf{M}}$ reduces the complete matrix equation for free harmonic plate motion to

$$\left[\frac{D}{ab}\bar{\mathbf{K}}_{el} - E\alpha T_0 h\bar{\mathbf{K}}_{th} - \omega^2\rho abh\bar{\mathbf{M}}\right]\{\mathbf{W}\} = 0, \tag{B.8}$$

which, divided through by D/ab $(= Eh^3/12(1-\nu^2))$, takes the completely dimensionless form

$$\left[\bar{\mathbf{K}}_{el} - T_{ND}\bar{\mathbf{K}}_{th} - \frac{\Omega^2}{AR^2}\bar{\mathbf{M}}\right]\{\mathbf{W}\} = 0. \tag{B.9}$$

T_{ND} and Ω are the non-dimensional temperature and frequency, respectively, defined by

$$T_{ND} = \frac{\alpha T_0 ab12(1-\nu^2)}{h^2} \tag{B.10}$$

and

$$\Omega = \sqrt{\frac{\omega^2\rho ha^4}{D}}. \tag{B.11}$$

References

[1] Lord Rayleigh, Theory of Sound (two volumes), 2nd Edition, Dover Publications, New York, 1877, 1945 re-issue.
[2] S. Timoshenko, D.H. Young, W. Weaver Jr., Vibration Problems in Engineering, 4th Edition, Wiley, New York, 1955.
[3] D.J. Mead, Free vibrations of self-strained assemblies of beams, Journal of Sound and Vibration 249 (2001) 101–127.
[4] A.W. Leissa, Vibration of Plates, U.S Government Printing Office, NASA SP-160, 1969.
[5] D.A. Simons, A.W. Leissa, Vibrations of rectangular cantilever plates subjected to in-plane acceleration loads, Journal of Sound and Vibration 17 (1971) 407–422.
[6] S.M. Dickinson, Lateral vibration of rectangular plates subject to in-plane stresses, Journal of Sound and Vibration 16 (1971) 465–472.
[7] C. Mei, T.Y. Yang, Free vibrations of finite element plates subjected to complex middle-plane force systems, Journal of Sound and Vibration 23 (1972) 145–156.
[8] D.J. Dawe, Comments on "Free vibrations of finite element plates subjected to complex middle-plane force systems", Journal of Sound and Vibration 28 (1973) 759–763.
[9] R.E.D. Porter Goff, The effect of self-equilibriating stresses on the natural frequencies of a free-free rectangular plate, Journal of Sound and Vibration 47 (1976) 85–94.
[10] M.M. Kaldas, S.M. Dickinson, Vibration and buckling calculations for rectangular plates subject to complicated in-plane stress distributions by using numerical integration in a Rayleigh–Ritz analysis, Journal of Sound and Vibration 75 (1981) 151–162.
[11] M.M. Kaldas, S.M. Dickinson, The flexural vibration of welded rectangular plates, Journal of Sound and Vibration 75 (1981) 163–178.
[12] C.D. Bailey, Vibration of thermally stressed plates with various boundary conditions, American Institute of Aeronautics and Astronautics Journal 11 (1973) 14–19.
[13] E.F.F. Chladni, Entdeckungen über die Theorie des Klanges, Leipzig, 1787.
[14] Lord Rayleigh, On the nodal lines of a square plate, Philosophical Magazine, Series 4, 46 (1873) 304.
[15] M.D. Waller, Concerning combined and degenerate vibrations of plates, Acustica 3 (1953) 370–374.
[16] D.J. Johns, Thermal Stress Analysis, Pergamon Press, Oxford, 1965.
[17] J.R. Przemieniecki, Thermal stresses in rectangular plates, Aeronautical Quarterly 10 (1959) 65–78.
[18] S.F. Bassily, S.M. Dickinson, The plane stress problem for rectangular regions treated using functions related to beam flexure, International Journal of Mechanical Sciences 19 (1977) 639–650.
[19] K. Rama Rao, D.J. Johns, Some thermal stress analyses for rectangular plates, Journal of the Aeronautical Society of India 13 (1961) 99.
[20] S. Timoshenko, Theory of Elastic Stability, 1st Edition, McGraw-Hill, New York, 1936.
[21] A. Lemke, Experimentelle Untersuchungen zur W. Ritzschen Theorie der transversalschwingungen quadratischer Platten, Annal Physik 86 (1928) 717–750.
[22] G.B. Warburton, The vibration of rectangular plates, Proceedings of the Institute of Mechanical Engineers, Series A 168 (1954) 371–384.
[23] G.B. Warburton, The Dynamical Behaviour of Structures, 2nd Edition, Pergamon Press, Oxford, 1976.
[24] C.D. Bailey, Modal coupling in thermally stressed plates, Journal of Aircraft 7 (1970) 557–562.
[25] A.W. Leissa, The free vibration of rectangular plates, Journal of Sound and Vibration 31 (1973) 257–293.
[26] S. Iguchi, Die Eigenschwingungen und Klangfiguren der vierseitig freien rechteckigen Platte, Ingenieur-Archiv 21, Ser. 303 (5–6) (1958) 304–322.
[27] N.S. Bardell, Free vibration analysis of a flat plate using the hierarchical finite element method, Journal of Sound and Vibration 151 (1991) 263–289.
[28] D.C. Johnson, R.E.D. Bishop, The Mechanics of Vibration, 1st Edition, Cambridge University Press, Cambridge, 1960.